Tellus (1990), *42A*, 520–530

On the effects of horizontal resolution and diffusion in a two-layer general circulation model with a zonally symmetric forcing

By ERIK ELIASEN, *Geophysical Institute, University of Copenhagen, Haraldsgade 6, DK-2200 Copenhagen N, Denmark* and LEIF LAURSEN, *Danish Meteorological Institute, Lyngbyvej 100, DK-2100 Copenhagen Ø, Denmark*

(Manuscript received 28 August 1989; in final form 4 December 1989)

ABSTRACT

The general circulation of a two-layer spectral model with a simple symmetrical forcing is determined from long-term integrations. It is found that the zonal as well as the meridional mean flow is clearly influenced by the horizontal resolution of the model. Related to that, it is also found that the meridional eddy transport of momentum is increased significantly by an increase of the horizontal resolution. As a main result of the present study, it is demonstrated, that the response of the model to an increase of the horizontal resolution can also be obtained to a considerable extent by using a suitable, strongly scale-dependent, linear diffusion in the model. Considering especially the spectral distribution of kinetic energy, it is found that an increase of the horizontal resolution as well as the use of a selective horizontal diffusion on the smaller scales results in a significant increase of the eddy kinetic energy on the large scales connected with an enhancement of the baroclinicity of the zonal mean flow. As to be expected, the effect of increasing horizontal resolution or the scale selective diffusion is also to decrease the kinetic energy on the smaller scales, with the result that the energy spectrum is approaching a -3-power law for a wider range of wavenumbers.

1. Introduction

In a recent paper by Laursen and Eliasen (1989), the important effect of lateral diffusion in an atmospheric general circulation model was pointed out. Generally lateral diffusion terms are introduced into the model equations in order to prevent spectral blocking with the argument that the lateral diffusion represents the effect of the unresolved horizontal scales on the explicitly predicted scales. In accordance with such considerations, it was found from numerical experiments with the model that it is possible to use a strongly scale-dependent linear diffusion in such a way, that the model simulates very closely the observed kinetic energy spectrum for the medium and smaller scales. Furthermore, it was found that an increase of the diffusion on the smallest scales results not only in a decrease of kinetic energy on those scales, as to be expected, but also in a significant increase of the kinetic energy on the larger scales.

The purpose of the study was to consider the possibility of reducing systematic errors (climate drift) of a medium resolution model by using different parameterizations of some of the physical processes entering the model. The model was a version of the first spectral model developed at European Centre for Medium Range Weather Forecasts and it was used with 9 levels in the vertical, and a horizontal triangular truncation with maximum total wavenumber 31. However, in order to study the effect of horizontal resolution and its relation to lateral diffusion it seems desirable to use a simple general circulation model without complicated formulations of physical processes and without any complicated influence from orography and land–ocean contrasts. Thus, in the present paper, the effects connected with the horizontal resolution as well as the lateral diffusion are considered by using a simple two-layer general circulation model with a homogeneous surface and a very simple forcing and dissipation.

From the numerical experiments with the present model, it turns out that an increase of horizontal resolution as well as the use of a strongly scale-selective horizontal diffusion cause in a quite similar way a significant growth of the eddy activity on the large scales. This growth is very pronounced for the meridional eddy momentum flux which further influences the mean meridional circulation and the mean zonal flow.

2. The model

The general circulation simulations considered are obtained from long-term integrations of a simple two-layer model quite similar to the model used by Eliasen (1982). Pressure p is used as the vertical coordinate and the vertical structure of the model is illustrated in Fig. 1. As usual ω denotes the individual time derivative of pressure, dp/dt. In consideration of the general crudeness of the model, it seems reasonable to use the condition $\omega = 0$ at $p = 1000$ hPa, as an approximate lower boundary condition. Similarly it is assumed that $\omega = 0$ at $p = 200$ hPa, which may be considered as a reflection of the stable stratification of the lower stratosphere. Together the two boundary conditions imply that the vertically integrated divergence of the flow is equal to zero, which means that the external gravity waves are excluded. With the conventional notation, the equation of motions may be written

$$\frac{\partial u_i}{\partial t} + u_i \frac{\partial u_i}{a \cos\phi\, \partial\lambda} + v_i \frac{\partial u_i}{a\, \partial\phi} - \frac{\operatorname{tg}\phi}{a} u_i v_i + \omega_i \frac{u_3 - u_1}{\Delta p} - f v_i + \frac{\partial \Phi_i}{a \cos\phi\, \partial\lambda} = (F_\lambda)_i$$

$$\frac{\partial v_i}{\partial t} + u_i \frac{\partial v_i}{a \cos\phi\, \partial\lambda} + v_i \frac{\partial v_i}{a\, \partial\phi} - \frac{\operatorname{tg}\phi}{a} u_i^2 + \omega_i \frac{v_3 - v_1}{\Delta p} + f u_i + \frac{\partial \Phi_i}{a\, \partial\phi} = (F_\phi)_i, \quad (1)$$

with the index $i = 1$ and 3 referring to the pressure levels p_1 and p_3, respectively. F_λ and F_ϕ represent the components of the frictional force $\boldsymbol{F}$ given by

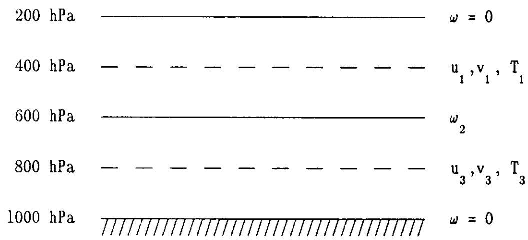

Fig. 1. The vertical structure of the two-layer model.

$$\boldsymbol{F}_1 = -k_d(\boldsymbol{v}_1 - \boldsymbol{v}_3), \quad \boldsymbol{F}_3 = k_d(\boldsymbol{v}_1 - \boldsymbol{v}_3) - k_s |\boldsymbol{v}_s| \boldsymbol{v}_s, \quad (2)$$

where the second term in the expression for $\boldsymbol{F}_3$ represents the surface frictional force. The wind vector $\boldsymbol{v}_s$ at the surface is introduced as $\boldsymbol{v}_s = \boldsymbol{v}_3 - \frac{1}{3}\boldsymbol{v}_1$. The constant values $k_d = 2 \cdot 10^{-6}\ \mathrm{s}^{-1}$ and $k_s = 8 \cdot 10^{-7}\ \mathrm{m}^{-1}$ are used. The equation of continuity together with the approximate boundary conditions for ω may be written

$$\frac{\omega_2}{\Delta p} = -\nabla \cdot \boldsymbol{v}_1 = \nabla \cdot \boldsymbol{v}_3 = -\nabla^2 \chi, \quad \omega_1 = \omega_3 = \tfrac{1}{2}\omega_2. \quad (3)$$

The hydrostatic equation is expressed as $\phi_1 - \phi_3 = c_p(r_3 - r_1)\theta_2$ and, energetically consistent with this, the thermodynamic equation is used in the form

$$\frac{\partial T_i}{\partial t} + u_i \frac{\partial T_i}{a \cos\phi\, \partial\lambda} + v_i \frac{\partial T_i}{a\, \partial\phi} - r_i \sigma \frac{\omega_2}{\Delta p} = \frac{Q_i + D_i}{c_p}, \quad (4)$$

where

$$r = \frac{T}{\theta} = \left[\frac{p}{p_0}\right]^{R/c_p}, \quad \theta_2 = \tfrac{1}{2}(\theta_1 + \theta_3),$$

$$\sigma = \tfrac{1}{2}(\theta_1 - \theta_3),$$

with $p_0 = 1000$ hPa. Q_i denotes the non-frictional heating rates per unit mass and the heating terms due to dissipation are defined as

$$D_1 = \tfrac{4}{5} k_d (\boldsymbol{v}_1 - \boldsymbol{v}_3)^2,$$

$$D_3 = \tfrac{1}{5} k_d (\boldsymbol{v}_1 - \boldsymbol{v}_3)^2 + k_s |\boldsymbol{v}_s| \boldsymbol{v}_s \cdot \boldsymbol{v}_3. \quad (5)$$

The model is forced by the expressions

$$\frac{Q_1}{c_p} = E\{\varepsilon C s(\mu) + a_3 \overline{T}_3^4 - b_1 \overline{T}_1^4\} + B,$$

$$\frac{Q_3}{c_p} = E\{(1-\alpha(\mu))Cs(\mu) - b_3 \overline{T}_3^4 + a_1 \overline{T}_1^4\} - B, \tag{6}$$

where $\mu = \sin\phi$, and the bar denotes a zonal mean. The simple form of the expressions is argued by Eliasen (1982) on the basis of the assumption of heat balance at the surface of the earth. Further, it is assumed that the surface is homogeneous except for a prescribed latitudinal variation of the term $(1-\alpha(\mu))$ expressing mainly the albedo effect of the mean ice and snow cover. In the present application, $\alpha(\mu) = 0.37 + 0.28\mu^4$. The fraction of the solar radiation absorbed in the upper layer ε is given the value 0.07. The term $s(\mu)$ denotes the annual average fraction of incident solar flux received at the latitude μ, and for $s(\mu)$, the Legendre polynomials expansion given by Coakley (1979) is used. The temperature dependence of the long-wave radiation terms is simplified by using only zonal mean values of T, and the following values of the constants are used $a_1 = 0.00$, $a_3 = 0.10$, $b_1 = 0.57$ and $b_3 = 0.42$. The coefficient C is proportional to the intensity of the solar radiation and with the normal value of the solar constant, $C = 6.0 \cdot 10^9$ K^4. Finally, the value $1.2 \cdot 10^{-9}$ K^{-3} is used for E. A simple convective adjustment parameterization is introduced in the model by the term

$$B = \begin{cases} k_T(\overline{T}_3 - \overline{T}_1 - \Gamma) & \text{if } \overline{T}_3 - \overline{T}_1 > \Gamma \\ 0 & \text{if } \overline{T}_3 - \overline{T}_1 < \Gamma, \end{cases} \tag{7}$$

with the values $\Gamma = 31$ K and $k_T = 5.0 \cdot 10^{-6}$ s^{-1}.

The model described briefly in the foregoing was integrated numerically by using the spectral method in the form developed by Bourke (1974). The horizontal velocity vector is expressed by the stream function ψ and the velocity potential χ, and the equations of motions (1) are replaced by the vorticity and divergence equations. As dependent variables, the model then contains 5 scalar variables ψ_1, ψ_3, χ, T_1, and T_3, which are described by truncated series of spherical harmonics with zonal wavenumber m and total wavenumber n. The model may be integrated numerically for the whole globe as well as for a single hemisphere by assuming symmetry about the equator. In some of the numerical experiments, especially those with high horizontal resolution, the spectral representation is restricted to the symmetrical case, which implies that T_1, T_3 and χ are even functions and ψ_1 and ψ_3 odd functions about the equator. The representation of the fields is truncated by $m \leqslant M$ and in the symmetrical case by $n \leqslant M$ for the variables which are even and $n \leqslant M+1$ for the variables which are odd about the equator. With this truncation in the symmetrical case, each of the variables have a horizontal resolution with the same number of degrees of freedom. In the general non-symmetrical case, the truncation $m \leqslant M$ and $n \leqslant M+1$ has been used.

The time integration was performed by using the semi-implicit method with the time step varying from 1 h to $13\frac{1}{3}$ min for the lowest ($M = 36$) and highest ($M = 72$) horizontal resolutions, respectively. The integrations were started from a state at rest and with the constant temperature values $T_1 = 250$ K and $T_3 = 275$ K. Due to the symmetry of the heating function $s(\mu)$ in eq. (4), the temperature fields will be symmetrical with respect to the axis of the earth as well as with respect to the equator. The same will be the case for the motion fields, which will develop. After 30 days of integration, time variations with longitude are introduced by imposing small random perturbations in the temperature field. Due to the baroclinic instability of the zonal flow, wave motions will develop and the eddy kinetic energy will increase over a period of about 20 days to a certain mean value upon which are superimposed rather small irregular fluctuations, corresponding rather well with observed conditions.

If the initial perturbations of the temperature field are introduced as being symmetrical with respect to the equator, the subsequent temperature and motion fields must be restricted to this symmetry. By using the transform method in the global spectral model, an integration which is initialized symmetrical will yield asymmetric perturbations arising from round-off errors in the pole-to-pole quadrature, which means that the symmetry may be maintained only by using the hemispheric spectral representation. If, on the other hand, the temperature perturbations are not restricted by any symmetry in the global representation, the eddy motions must also develop without symmetry, but still the long-term statistics will be symmetrical with respect to the equator and as a matter of fact be the same or at

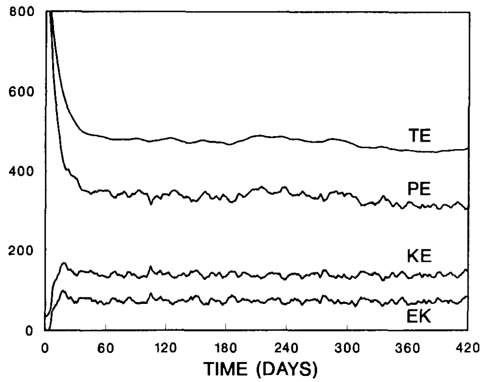

Fig. 2. Time series of global averaged energy quantities per unit mass (J kg^{-1}) for the symmetrical M36 integration without horizontal diffusion. Eddy kinetic energy EK, the total kinetic energy KE, the potential energy PE and the total energy TE.

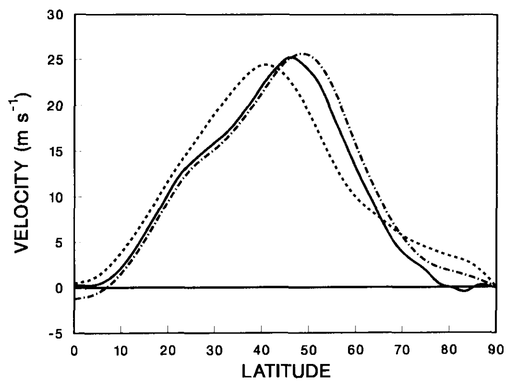

Fig. 3. Time-averaged from days 180–360 of the mean zonal wind (m s^{-1}) at the upper level for M72 without horizontal diffusion (solid), M36 without horizontal diffusion (dashed) and M36 with horizontal diffusion, $A = 2 \cdot 10^{-4}$ s^{-1}, (dash-dotted).

least very close to the statistics of integrations with strictly symmetrical motions.

The development and fluctuations of global mean quantities of energy per unit mass are shown in Fig. 2 for the first 420 days of integration after the imposing of perturbations. The integration is for the symmetrical case and with resolution $M = 36$ (in the following denoted M36), and the figure shows the values of the eddy kinetic energy, the total kinetic energy, the total potential energy and finally the sum of kinetic and total potential energy. The total potential energy is computed as

$$\mathrm{PE} = c_{\mathrm{p}} \left[\frac{(T_1 - T_3)}{2} - 246.5 \right],$$

where the square bracket denotes a mean value over the sphere. From the figure, it is seen that the fluctuations of the kinetic energy are mainly fluctuations of the eddy part and furthermore, it is seen that the fluctuations of the total potential energy are to some extent of the same size (but opposite sign) as the fluctuations of the kinetic energy, leading to the rather smooth curve for the total energy.

3. Results of experiments

One of the basic quantities describing the general circulation of the model is the long-term mean flow, which for the simple model used here will be symmetrical with respect to the axis of the earth. Actually, the motion contains large-scale low-frequent waves to such a degree that it is necessary to use more than 90 days mean values in order to obtain the purely symmetric mean flow. Fig. 3 shows the mean zonal flow as a function of latitude at the upper level obtained as 180-day mean values for the two different symmetrical resolutions M36 and M72. It is seen that the increased resolution implies an essential change with a displacement of the maximum of the westerly flow towards the pole. In both cases, the model has been integrated without any horizontal diffusion. Quite generally, however, the use of horizontal diffusion in numerical integration models is based on the assumption that the diffusion may approximately represent the effect of the unresolved scales on the explicitly described scales. From this assumption, it should be expected that the change of the zonal flow similar to that occurring when the horizontal resolution is increased from M36 to M72 could be obtained by introducing a suitable horizontal diffusion in the model with the low resolution. In the paper by Laursen and Eliasen (1989), the usefulness of a simple linear strongly scale-dependent diffusion was demonstrated and a quite similar diffusion formulation is introduced in the equations of vorticity, divergence and temperature of the present model. Formally, the vorticity equation may be written

$$\frac{\partial \xi_{m,n}}{\partial t} = R_{m,n} + F_{m,n}, \tag{8}$$

where $\xi_{m,n}$ is the spectral component of the vorticity. $F_{m,n}$ represents the lateral diffusion and $R_{m,n}$ all other terms. Generally, the scale dependency in terms of the total wavenumber n may be written

$$F_{m,n} = -A_n \xi_{m,n}, \tag{9}$$

where A_n is increasing more or less with n. In order to have the possibility to increase the damping on the smaller scales without a simultaneous increase of the damping of the larger scales, the following form as introduced by Boer et al. (1984) is used:

$$A_n = \begin{cases} A\left(\dfrac{n-n_*}{M}\right)^2 & n > n_* \\ 0 & n \leqslant n_*, \end{cases} \tag{10}$$

where A is a constant. Taking $n_* = \frac{2}{3}M$, the value of A_n for $n = M$ will be $\frac{1}{9}A$, independent of M. With the form of the horizontal diffusion given by eqs. (8), (9) and (10), the diffusion will be an exponential damping for each scale represented by n with the e-folding decay time equal to $9/A$ for the scale M. In order to see the effect of the lateral diffusion, several numerical experiments have been performed combining the different horizontal resolutions with different strengths of the diffusion. In Fig. 3, the dotted curve shows the mean zonal flow resulting from the integration of the model with the horizontal resolution M36 and the strength of the lateral diffusion given by $A = 2 \cdot 10^{-4}$ s^{-1} corresponding to the e-folding decay time 12.5 h for the scale M. It is clearly seen from the figure that the effect of introducing the lateral diffusion is quite similar to an increase of the horizontal resolution. Actually, by choosing the weaker diffusion with $A = 1 \cdot 10^{-4}$ s^{-1}, a mean zonal flow is obtained which is quite close to the case with resolution M72 and no horizontal diffusion.

The changes of the long-term mean zonal flow shown in Fig. 3 must occur in accordance with the long-term momentum balance equation, which for the present model, may be obtained at level p_1 from eqs. (1), (2) and (3) in the form

$$\bar{v}_1(\bar{\xi}_1 + f) + \frac{\overline{\omega_2}}{\Delta p}\frac{\overline{u_1} - \overline{u_3}}{2} - \frac{\partial(\overline{u_1' v_1' \cos^2\phi})}{a\cos^2\phi\,\partial\phi}$$
$$- \overline{\frac{\omega_2'}{\Delta p}\frac{u_1' + u_3'}{2}} = k_{\mathrm{d}}(\bar{u}_1 - \bar{u}_3), \tag{11}$$

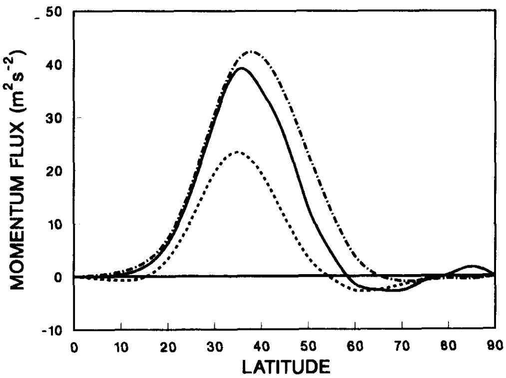

Fig. 4. Time-averaged from days 180–360 of $\overline{u_1' v_1'}\cos\phi$ (m^2 s^{-2}) for M72 without horizontal diffusion (solid), M36 without horizontal diffusion (dashed) and M36 with horizontal diffusion, $A = 2 \cdot 10^{-4}$ s^{-1}, (dash-dotted).

where zonal mean values are indicated by a bar and deviations from a zonal mean value by primed letters. From the model data, it is found just as for the general circulation of the real atmosphere, that the horizontal eddy momentum flux $\overline{u'v'}\cos\phi$ plays an essential role in maintaining the balance of the zonal flow, and moreover, it is found that the eddy momentum flux of the model is strongly influenced by the horizontal resolution and by the horizontal diffusion as shown by Fig. 4. It is clearly seen from the figure that the eddy momentum flux is increased by a factor of 2 by increasing the horizontal resolution of the model from M36 to M72 for integrations without horizontal diffusion. Similarly, the inclusion of horizontal diffusion in the M36 resolution results in an increase of the eddy momentum flux to the level of the high-resolution experiment.

The insufficient eddy momentum flux obtained with low resolution general circulation models has been discussed by Palmer et al. (1986) and with the Meteorological Office 11-layer GCM, it was demonstrated that with 5° latitude and 7.5° longitude resolution, the eddy momentum flux in 250 hPa was only about half that obtained with the same model used with 2.5° latitude and 3.75° longitude horizontal resolution. The result is consistent with findings from other GCMs as discussed in the paper referred to. The descriptions of lateral diffusion in general circulation models vary, but generally they are less scale

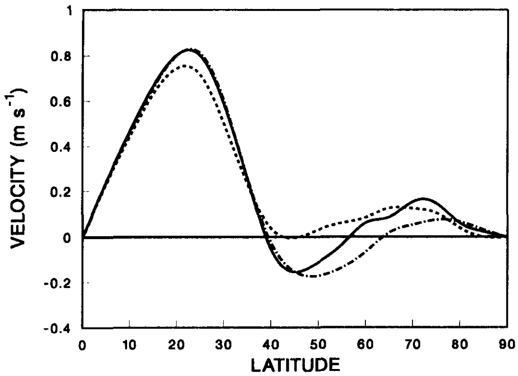

Fig. 5. Time-averaged from days 180–360 of $\bar{v}_1$ (m s^{-1}) for M72 without horizontal diffusion (solid), M36 without horizontal diffusion (dashed) and M36 with horizontal diffusion, $A = 2 \cdot 10^{-4}$ s^{-1}, (dash–dotted).

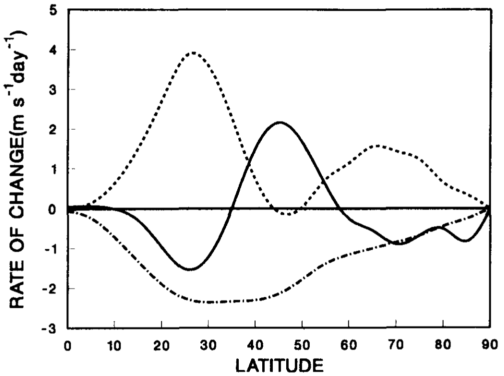

Fig. 6. Time-averaged from days 180–360 of the contributions to the rate of change of the mean zonal wind at the upper level for M36 without horizontal diffusion, from the convergence of eddy momentum flux (solid), the mean meridional circulation (dashed) and the vertical diffusion (dash–dotted).

selective and weaker on the small scales than the formulation used in the present model. The Canadian Climate Centre general circulation model uses a formulation of lateral diffusion (Boer et al., 1984) as the one used in the present model, and actually the dependence on horizontal resolution of the simulated climate with the Canadian model is quite modest (Boer and Lazare, 1988).

The other dynamical factor determining the mean zonal flow is the convergence of momentum flux connected with the mean meridional circulation as represented by the first two terms of eq. (11). In the simple two-layer formulation, the mean meridional circulation is described by $\bar{v}_1 = -\bar{v}_3$ and values of $\bar{v}_1$ obtained from numerical experiments are shown in Fig. 5 as a function of latitude. It is seen that the direct circulation (Hadley cell) in the tropical and subtropical area is increased somewhat by introducing the horizontal diffusion in the M36 resolution and also by going from the M36 to the M72 resolution without horizontal diffusion. Furthermore, in the extra-tropical area, the mean meridional circulation is influenced by the effects of horizontal resolution or horizontal diffusion which is likely to be a manifestation of the induced meridional circulation connected with the baroclinic waves in order to maintain the quasi-geostrophic and hydrostatic balance of the zonal flow. The momentum balance expressed by eq. (11) is illustrated in Fig. 6 for the M36 integration without horizontal diffusion. The first two terms of eq. (11) represent together the contribution of the convergence of momentum transport by the meridional circulation and is given by the dotted curve. It should be noted that almost the whole contribution comes from the Coriolis term $\bar{v}_1 \cdot f$ and that in the vertically integrated momentum balance equation, this term is cancelled by the term $\bar{v}_3 \cdot f$. The contribution from the convergence of horizontal eddy momentum transport is seen from the full drawn curve, whereas the values of

$$\overline{\frac{\omega_2'}{\Delta p} \frac{u_1' + u_3'}{2}}$$

from the vertical eddy transport are quite small and not shown in the figure. Finally, the balance is obtained from the dash–dotted curve giving the sink of momentum due to the vertical diffusion term $-k_d(\bar{u}_1 - \bar{u}_3)$. In the same way, Fig. 7 illustrates the momentum balance for the integration with the M36 resolution and with the horizontal diffusion with $A = 2 \cdot 10^{-4}$ s^{-1}. It is seen that an effect of the use of horizontal diffusion is to significantly increase the convergence of the horizontal eddy momentum transport in middle latitudes, as may also be deduced immediately from Fig. 4. Simultaneously, however, there is a compensating sink of momentum in middle latitudes due to the meridional circulation, well in agreement with the non-acceler-

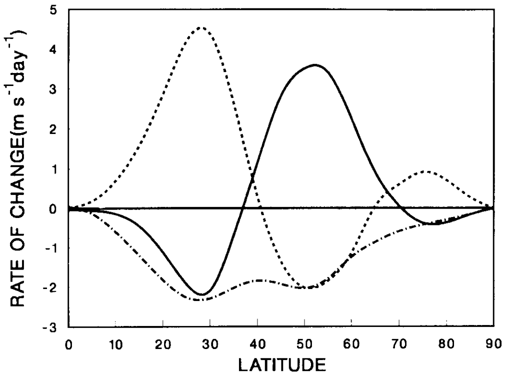

Fig. 7. As Fig. 6 but for M36 with horizontal diffusion, $A = 2 \cdot 10^{-4}$ s^{-1}.

ation theorem based on the theory of the induced meridional circulation, Charney and Drazin (1961).

The increase of the horizontal eddy momentum flux resulting from an increase of the horizontal resolution or from the use of the horizontal diffusion seems to be connected with a parallel increase of the eddy kinetic energy on the large scales. The distribution of the kinetic energy on the different horizontal scales is obtained by writing the mean values over the sphere of the kinetic energy per unit mass of rotational part of the flow as the sum of the kinetic energy of the zonal flow ZK and the eddy kinetic energy K, where

$$K = \sum_{m>0} \sum_{n} K_{m,n} \tag{12}$$

with

$$K_{m,n} = \frac{1}{2} \frac{n(n+1)}{a^2} |\psi_{m,n}|^2 \quad \text{for } m > 0 \tag{13}$$

the kinetic energy of the motion described by the spherical harmonic component of the stream-function. Besides the two-dimensional spectral distribution given by $K_{m,n}$, it is also of interest to consider the one-dimensional spectrum defined by

$$K_n = \sum_{m>0} K_{m,n}, \tag{14}$$

where K_n is the sum of kinetic energy of all wave components with the same spherical harmonic index n.

The influence of the horizontal resolution and of the horizontal diffusion is illustrated in Table 1, giving ZK and summarized values of K_n. From the values, it is seen that the increase of the resolution from M36 to M72 causes a significant increase of kinetic energy on the large scales, $n = 1$–13 and also a significant decrease of the kinetic energy on the medium and smaller scales, $n = 14$–25 and $n = 26$–37. Furthermore, it is seen from the table that the use of horizontal diffusion has a quite similar effect, also in the high-resolution case. The last row in the table contains the values of $C(P, K)$ which are the long-term mean values of the transformation per unit mass of total potential energy into kinetic energy, which in the simple two-layer model may be expressed as

$$C(P, K) = -\frac{1}{2} \left[(\phi_1 - \phi_3) \frac{\omega_2}{\Delta p} \right]. \tag{15}$$

Table 1. *Kinetic energy values ($J\ kg^{-1}$) and the conversion $C(P, K)$ ($J\ kg^{-1}\ day^{-1}$)*

		M36		M72	
		$A = 0$	$A = 3 \cdot 10^{-4}$ s^{-1}	$A = 0$	$A = 3 \cdot 10^{-4}$ s^{-1}
$\sum K_n$	$n = 1$–13	22.7	31.5	27.3	36.9
	$n = 14$–25	21.5	12.3	14.2	13.6
	$n = 26$–37	13.7	1.8	4.6	2.9
	$n = 38$–73	—	—	7.9	1.7
K		57.9	45.6	53.9	55.0
ZK		55.1	54.6	52.3	49.0
$C(P, K)$		31.8	31.4	31.8	31.5

It is to be remarked from the table that $C(P, K)$ is independent of the horizontal resolution and that the effect of horizontal diffusion upon $C(P, K)$, if any, is quite small. Furthermore, it may be noted that the value of $C(P, K)$ obtained from the model is of the same magnitude as the values known for the real atmosphere. From the expressions eq. (5) used for the dissipation terms in the thermodynamic eq. (4), it follows that in the model with no horizontal diffusion, there is a long-term balance between $C(P, K)$ and the total dissipation $D = \frac{1}{2}[D_1 + D_3]$, from which follows the vanishing of the long-term mean value of the non-frictional heating $[Q_1 + Q_3]$. With the use of horizontal diffusion in the model, this is not the case and actually for the integration M36 with $A = 3 \cdot 10^{-4}$ s^{-1} as listed in Table 1, D is 9.1% smaller than $C(P, K)$.

A somewhat more detailed picture of the effects of horizontal resolution and horizontal diffusion upon the spectral distribution of kinetic energy may be obtained by considering the one-dimensional spectral curves K_n shown in Fig. 8. It is seen that an increase of horizontal resolution from M36 to M72 in the integration without horizontal diffusion implies a decrease of the spectral values for $n > 12$ and an increase for the larger scales with $n < 12$. Furthermore, it is seen that the use of horizontal diffusion in the M36 resolution has a quite similar effect as the increase of the horizontal resolution. The spectral distribution of kinetic energy in the atmosphere has been studied quite intensively during the last 25 years from analysis of observational data as well as from theoretical considerations. A recent account of the problem representing both the empirical and the theoretical part is given by Boer and Shepherd (1983). A special interest has been directed toward the existence of a certain subrange in n, where the kinetic energy should follow a -3 power law as found from observed data by Wiin-Nielsen (1967). From Fig. 8, it appears that the effect of increasing the horizontal resolution is actually to change the spectral curve towards a -3 power decrease for values of n larger than 12. The figure also clearly demonstrates that it is possible to obtain the -3 power law in the M36 resolution by using the horizontal diffusion with a suitable value of the coefficient A. The same was found for a more realistic general circulation model in the paper by

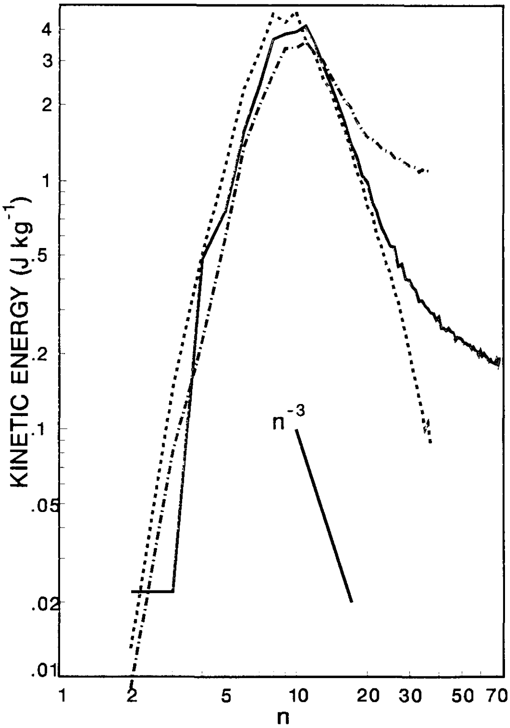

Fig. 8. Time-averaged from days 180–360 of the energy spectra K_n (J kg^{-1}) at the upper level for M72 without horizontal diffusion (solid), M36 without horizontal diffusion (dash–dotted) and M36 with horizontal diffusion, $A = 2 \cdot 10^{-4}$ s^{-1}, (dashed).

Laursen and Eliasen (1989), where also the spectrum at the 500 hPa level is compared with the spectrum obtained from observed data.

The approximate n^{-3} behavior of the kinetic energy spectrum in a certain subrange of n is generally considered as a consequence of the fact that the atmospheric flow is very nearly two-dimensional. From the equilibrium theory of two-dimensional homogeneous isotropic turbulence, it follows (Kraichnan, 1967) that an initial enstrophy-cascading subrange will be connected with a -3 power law of the kinetic energy spectrum. Alternatively, Charney (1971) presented a theory for the large-scale atmospheric turbulence based on the quasi-geostrophic character of the flow. From this theory, it also follows that the kinetic energy must exhibit a -3 power law in a certain subrange, but moreover, it also follows that the same must be the case for the

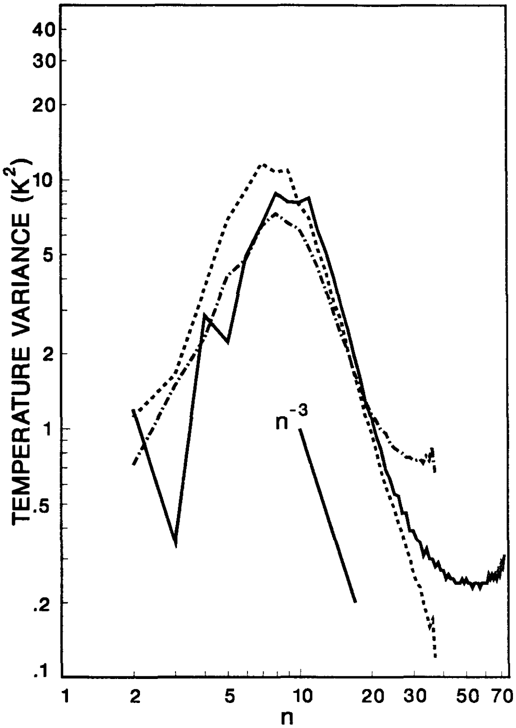

Fig. 9. Time-averaged from days 180–360 of the spectra of the temperature variance (K^2) at the lower level for M72 without horizontal diffusion (solid), M36 without horizontal diffusion (dash–dotted) and M36 with horizontal diffusion, $A = 2 \cdot 10^{-4}$ s^{-1}, (dashed).

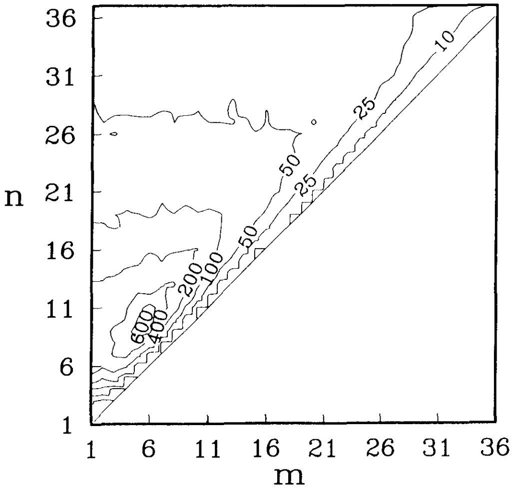

Fig. 10. Time-averaged from days 180–360 of the energy spectrum $K_{m,n}$ (10^{-3} J kg^{-1}) at the upper level for the global M36 without horizontal diffusion.

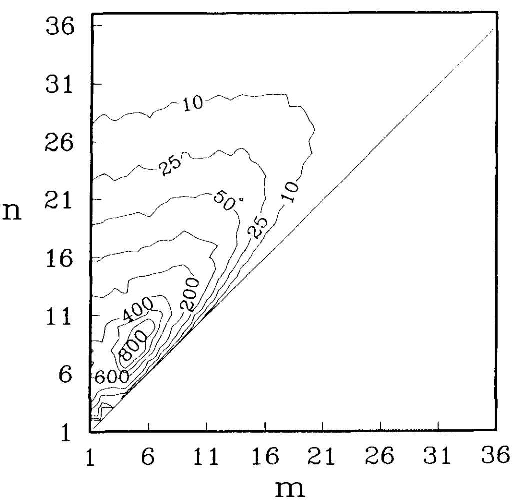

Fig. 11. Same as Fig. 10 but for M36 with horizontal diffusion, $A = 2 \cdot 10^{-4}$ s^{-1}.

available potential energy and thereby for the temperature spectrum. Spectra of the variance of the eddy part of the temperature field obtained from the present model are shown in Fig. 9. From the figure, it is clearly seen that there is a close approach to the -3 power decrease in a subrange of n with $n > 12$, and furthermore, that the approach becomes closer and the range of n extended when the resolution is increased from M36 to M72 and when the horizontal diffusion is included in the M36 integration.

The most detailed information about the spectral distribution of the kinetic energy is obtained, of course, by considering the two-dimensional spectrum $K_{m,n}$. In Figs. 10 and 11, the spectral distribution is shown by isopleths of $K_{m,n}$ for the global M36 representation without and with horizontal diffusion, respectively. In a similar way, the observed vertically-integrated spectral distribution of kinetic energy was presented and discussed in the paper by Boer and Shepherd (1983). As for the observed spectral distribution, Figs. 10 and 11 show that for $n > 12$, the isopleths are reasonably horizontal, apart from the drop of the values near the edge of the triangle. As pointed out by Boer and Shepherd, the condition that $K_{m,n}$ is independent of m is a necessary

Table 2. $K_{m,n}$ *(10^{-2} J kg^{-1}) at the upper level for the global M36 integration without horizontal diffusion*

12	25	24	30	29	28	44	41	44	30	19	7	2
11	22	30	28	27	39	54	68	51	29	8	2	
10	24	28	32	32	41	61	73	33	12	3		
9	25	30	28	46	53	69	66	16	4			
8	22	32	34	39	50	57	30	4				
7	23	30	26	43	48	24	6					
6	29	30	22	27	22	6						
5	15	15	10	14	4							
4	12	4	4	2								
3	6	1	1									
2	1	0										
1	0											
n/m	1	2	3	4	5	6	7	8	9	10	11	12

Table 3. $K_{m,n}$ *(10^{-2} J kg^{-1}) at the upper level for the global M36 integration with horizontal diffusion,* $A = 2 \cdot 10^{-4}$ s^{-1}

12	22	26	26	28	32	56	51	36	24	13	4	0
11	31	25	29	36	48	63	65	39	18	5	1	
10	34	35	57	67	84	114	54	20	8	1		
9	36	39	50	73	106	73	38	12	2			
8	67	42	66	90	118	63	14	2				
7	36	50	48	110	62	17	3					
6	43	51	47	58	28	4						
5	30	28	23	30	4							
4	30	8	9	4								
3	11	2	1									
2	1	0										
1	0											
n/m	1	2	3	4	5	6	7	8	9	10	11	12

condition for homogeneity and isotropy of the eddy motion. For each zonal wavenumber, the kinetic energy increases with n to a maximum value at n–m in the range 3–5 and from the maximum, the energy values decrease with n, most rapidly, of course, in the case with horizontal diffusion. The individual values in units of 10^{-2} J kg^{-1} of the energy spectrum for the largest scales with $n \leqslant 12$ are shown in Tables 2 and 3 for the same integration as in Figs. 10 and 11, respectively. From Table 2, it is seen that the largest values are 73 and 69 for the components $(m, n) = (7, 10)$ and $(6, 9)$. In the case with horizontal diffusion, the maximum values are 118 and 114 for the components $(5, 8)$ and $(6, 10)$, respectively, as seen from Table 3. By comparing the two-dimensional spectra of Figs. 10 and 11 as well as Tables 2 and 3, it is found that the effect of horizontal diffusion is to significantly increase the kinetic energy of rather few large-scale components essentially with $m \leqslant 6$ and $n \leqslant 12$. Thus, the kinetic energy of the component $(m, n) = (4, 7)$ is increased from 43 to 110 and for the component $(m, n) = (5, 8)$ from 50 to 118. For all components outside the range mentioned, the effect of horizontal diffusion is to decrease the kinetic energy and for all smaller scales with $n > 18$ the decrease is rather uniform around the value 3.5, except for the components near the edge of the triangle.

4. Concluding remarks

In the present paper, the effect of horizontal resolution and its relation to horizontal diffusion has been investigated by use of a simple two-layer model. It has been demonstrated that with this model, the eddy activity is strongly dependent on the horizontal resolution. The increased eddy activity in the experiments with high horizontal resolution has been shown to be apparent in the eddy momentum flux as well as in the level of eddy kinetic energy. Furthermore, it is demonstrated that with the use of a strongly scale-selective horizontal diffusion in the model with medium resolution, it is quite possible to obtain an increase of the eddy activity very similar to that obtained by the high resolution version of the model.

Considering a possible explanation of the striking increase of kinetic energy of the large-scale components connected with the use of horizontal diffusion, it should be noted that these large-scale components must be considered as those with the largest growth-rates due to baroclinic instability of the mean zonal flow. Actually, it is found that the baroclinicity of the mean temperature field is increased by increased horizontal diffusion perhaps due to a weaker meridional horizontal transport by the small-scale eddies. Thus, it is found that the difference of the mean temperature between latitudes 40° and 60° for the M36, resolution is increased from 12.4K in the case with no horizontal diffusion to 14.1K in the case with horizontal diffusion, with $A = 2 \cdot 10^{-4}$ s^{-1}. Another possible explanation of the increased eddy activity on the large scales connected with the horizontal diffusion could be that the kinetic energy is generally transferred from the larger baroclinic scales to smaller scales and that this transfer is reduced when the amplitudes of the smaller scales are kept down by the horizontal diffusion.

The increased eddy activity by application of the horizontal diffusion as found for the present model has also been demonstrated in a much more realistic general circulation model (Laursen and Eliasen, 1989). In that model, the lateral diffusion was applied on sigma-surfaces and it is not clear to what extent the realistic horizontal variation of physical forcing of the model interacts with the horizontal diffusion. In the present simple two-layer model, however, the homogeneous surface excludes all effects from orography and land–sea contrasts as possible explanations of the change in the eddy activity connected with resolution or horizontal diffusion.

REFERENCES

Boer, G. J. and Shepherd, T. G. 1983. Large-scale two-dimensional turbulence in the atmosphere. *J. Atmos. Sci. 40*, 164–184.

Boer, G. J., McFarlane, N. A., Laprise, R., Henderson, J. D. and Blanchet, J.-P. 1984. The Canadian Climate Centre spectral atmospheric general circulation model. *Atmosphere-Ocean 22*, 397–429.

Boer, G. J. and Lazare, M. 1988. Some results concerning the effect of horizontal resolution and gravity–wave drag on simulated climate. *J. of Climate 1*, 789–806.

Bourke, W. 1974. A multi-level spectral model. I. Formulation and hemispheric integrations. *Mon. Wea. Rev. 102*, 687–701.

Charney, J. G. 1971. Geostrophic turbulence. *J. Atmos. Sci. 28*, 1087–1095.

Charney, J. G. and Drazin, P. G. 1961. Propagation of planetary-scale disturbances from the lower into the upper atmosphere. *J. Geophys. Res. 66*, 83–109.

Coakley, J. A. 1979. A study of climate sensitivity using a simple energy balance model. *J. Atmos. Sci. 36*, 260–269.

Eliasen, E. 1982. Climate modeling using an equivalent meridional circulation. *Tellus 34*, 228–244.

Kraichnan, R. H. 1967. Inertial subranges in two-dimensional turbulence. *Phys. Fluids 10*, 1417–1423.

Laursen, L. and Eliasen, E. 1989. On the effects of the damping mechanisms in an atmospheric general circulation model. *Tellus 41A*, 385–400.

Palmer, T. N., Shutts, G. J. and Swinbank, R. 1986. Alleviation of a systematic westerly bias in general circulation and numerical weather prediction models through an orographic gravity wave drag parameterization. *Quart. J. R. Met. Soc. 112*, 1001–1039.

Wiin-Nielsen, A. 1967. On the annual variation and spectral distribution of atmospheric energy. *Tellus 19*, 540–559.